Revealing Significant Medial Structure in Polyhedral Meshes

Svetlana Stolpner Kaleem Siddiqi

Department of Computer Science,
Centre for Intelligent Machines
McGill University
Montréal, QC, H3A 2A7, Canada
{sveta, siddiqi}@cim.mcgill.ca

Abstract

Medial surfaces are popular representations of 3D objects in vision, graphics and geometric modeling. They capture relevant symmetries and part hierarchies and also allow for detailed differential geometric information to be recovered. However, exact algorithms for their computation from meshes must solve high-order polynomial equations, while approximation algorithms rarely guarantee soundness and completeness. In this article we develop a technique for computing the medial surface of an object with a polyhedral boundary, which is based on an analysis of the average outward flux of the gradient of its Euclidean distance function. This analysis leads to a coarse-to-fine algorithm implemented on a cubic lattice that reveals at each iteration the salient manifolds of the medial surface. We provide comparative results against a state-of-the-art method in the literature.

1. Introduction

Consider a region Ω in $\mathbb{R}^3$, with boundary B. Blum suggested that an intuitive representation of this region is one which makes its reflective symmetries explicit [4]. A formal definition that we adopt is the following

Definition 1.1. *The **medial surface** $\mathcal{MS}$ of Ω is the locus of centres of maximal spheres in Ω.*

Roughly speaking, $\mathcal{MS}$ is the set of points that are equidistant from at least two points of B. Figures 5, 6 and 7 present examples. Extracting the medial surface of Ω is reversible given that for each point of M one can note the radius of its maximal sphere.

It has been recently shown [7] that the differential geometry of Ω and its boundary B can be studied using the differential geometry of $\mathcal{MS}$. However, to make computational use of this relationship, it is necessary to first have a sound and complete algorithm for detecting the medial surface.

In 3D, the medial surface is composed of 2D sheets meeting along 1D seams and 0D junctions. When Ω is a polyhedron, the sheets are quadric surfaces, non-degenerate seams are intersections of 3 quadric surfaces, and non-degenerate junctions are intersections of 4 such surfaces. Exact computation of medial surfaces, even in the simple case of a polyhedron, requires the solution of equations of high algebraic degree. Consequently, it is reasonable to seek to approximate the medial surface.

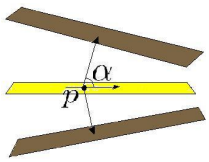

Figure 1. The object angle at a smooth medial point p is α.

Definition 1.2. *For a particular point p on a sheet of $\mathcal{MS}$, the **object angle** α is the angle made by the vector from p to any of its two closest points on B and the tangent plane to $\mathcal{MS}$ at p. Such a point p is called a **smooth medial point**.*

The concept of the object angle is illustrated in Figure 1. The idea that sections of medial surface with high object angle represent the most perceptually salient parts of an object's boundary is the basis of many techniques in the literature for removing "unwanted" sheets [1, 2, 10].

1.1. Previous Work

The problem of accurately computing the medial surface of a 3D solid represented by polygonal patches or point clouds has been extensively studied. Existing methods may be divided into the following categories: tracing algorithms, bisector methods for points distributed on the shape's boundary, and approaches based on spatial subdivision which detect singularities in the distance transform of the object boundary.

[5] presents a notable tracing algorithm that uses exact arithmetic to accurately compute the seam curves. It is able to compute the medial surface for polyhedra having several hundred faces.

[12, 13] compute a geometric directed graph, a "shock scaffold," whose nodes correspond to special medial points using exact bisector computations between node clusters. [2] approximates the medial surface by a triangulation of a subset of the vertices of the Voronoi diagram of points distributed appropriately on the surface of the solid. Research is carried out to prune sections of this medial surface to obtain a simpler reconstructed surface [21]. The task of pruning the medial surface for 3D objects, however, is quite complex [16].

[9] uses space subdivision to find the adjacency relationships between components of the generalized Voronoi diagram of 3D polyhedra. Subdivision continues until each cell contains one Voronoi vertex. [3] constructs a polyhedral approximation of the generalized Voronoi diagram for sites of various shapes under different metrics using an octree data structure. [22] uses spatial subdivision to approximate the generalized Voronoi diagram of a set of disjoint convex sites in any dimension. The cells kept by the algorithm are those whose vertices have different closest points on the boundary of the solid and are proven to intersect the Voronoi diagram. [10] uses spatial sampling to approximate the medial surface sections having a chosen object angle with axis-aligned facets. [20] extends this method to allow for preservation of homotopy type during simplification. In general, the spatial subdivision methods that perform distance computations between the cells and the boundary at a small number of locations are limited in that they cannot guarantee completeness in detecting all sections of the medial surface at any resolution.

[8, 18] study the shocks that arise when the boundary of an object is evolved according to a differential equation. In the continuum, these shocks correspond to the medial surface of the object. [8] considers a discretization of this notion to a square lattice for computing the medial axis of a 2D shape. [18] extends this work to a 3D voxelized object using approximate distances and coarse sampling. Both approaches, though applicable to shape matching [23], lack theoretical guarantees on the correctness of the results.

In this article we overcome these limitations by developing a criterion to detect provably accurate locations of medial sheets of polyhedra through recursive spatial subdivision. We provide a stronger guarantee than other subdivision methods about the sections of the medial surface that are retained.

We develop the necessary background in Sections 2 and 3, and the theory and implementation of our new algorithm, along with experimental results, in Sections 4, 5, and 6.

2. Continuous Case

Let B be the boundary of a closed orientable 3D object and $W(t)$ be a moving front. If t is the time parameter, then let $W(0) = B$. If we evolve $W(t)$ according to the equation of the grassfire flow $\frac{\partial W}{\partial t} = \hat{\mathbf{N}}$, where $\hat{\mathbf{N}}$ is the unit inward normal to $W(t)$, the shocks of $W(t)$ corresponding to two or more evolving fronts colliding comprise the medial surface of B.

Definition 2.1. *The **Euclidean distance transform** $D : \mathbb{R}^3 \rightarrow \mathbb{R}$ for a surface B is given by $D(p) = \chi(p) \inf_{q \in B} d(p, q)$, where $d(.,.)$ denotes the Euclidean distance and $\chi(p) = -1$ if p is outside or on B and 1 if p is inside B.*

The gradient of the distance transform $\nabla D : \mathbb{R}^3 \rightarrow \mathbb{R}^3$ is a vector field, with vectors inside B pointing away from B.

Observing that $\hat{\mathbf{N}} = \nabla D$ in the grassfire flow equation, the medial surface may be interpreted as the locus of those points for which ∇D is not uniquely defined, or where the Euclidean distance transform D is singular.

Our approach for detecting sections of the medial surface is to detect discontinuities in the vector field ∇D. In particular, we study the limiting behaviour of the average outward flux ($\mathcal{AOF}$) of ∇D through a shrinking neighbourhood S inside B [8].

The flux of ∇D through S with outward normal N_S is

$$\iint_S \nabla D \cdot N_S dS,$$

and can be interpreted as the degree to which the flow produced by ∇D is volume preserving.

As the region S shrinks to a point, the flux of ∇D through S tends to zero. However, the value of the average outward flux through S

$$\mathcal{AOF}(S) = \frac{\iint_S \nabla D \cdot N_S du dv}{\iint_S dS}$$

as S shrinks to a point is related to the object angle of the medial surface sheet, if any, passing through S.

smooth medial point	$\frac{1}{2}$
Y-branch seam point	$\frac{3}{4}$
6-junction point	$\geq \frac{1}{2}$
non-medial point	0

Table 1. Value of constant μ for a spherical region for different kinds of points [6].

Whenever $\mathcal{MS}$ passes through S or ∇D is discontinuous, we must adopt this special form of the Divergence Theorem [8]:

$$\iint_S \nabla D \cdot N_S dS = \iiint_{\mathbf{S}} div(\nabla D) d\mathbf{S} - 2 \iint_C \nabla D \cdot N_S dS,$$

where $\mathbf{S}$ is the solid sphere with boundary S and C is the region of $\mathcal{MS}$ intersected by the interior of S. When considering the $\mathcal{AOF}$ of a region S shrinking to a point x, the first term on the right side tends to zero, while the second term does not:

$$\begin{aligned} \lim_{area(S)\to 0} \frac{\iint_S \nabla D \cdot N_S dS}{\iint_S dS} &= -2 \frac{\iint_C \nabla D \cdot N_S dS}{\iint_S dS} \\ &\leq -2 \frac{\iint_C dS}{\iint_S dS} \min(\nabla D \cdot N_S) \\ &= -\mu \sin(\min_i \alpha_i). \end{aligned}$$

The α_i are the object angles of the medial sheets meeting at x. The values of μ are summarized in Table 1 for different kinds of points inside Ω. For smooth medial points, C is just a circle with the same radius r as S, so μ is $2 \cdot \frac{\pi r^2}{4\pi r^2} = \frac{1}{2}$.

3. Discrete Case

It has been proposed [8, 18] that the above continuous measure of the $\mathcal{AOF}$ on a convex, closed 2D surface S may be discretized as follows:

$$AOF_S(\nabla D) = \frac{\sum_{i=1,\ldots,N} \nabla D(p_i) \cdot N_S(p_i) d\mathbf{a}_i}{Area(S)},$$

where p_i are points sampled uniformly on S and $d\mathbf{a}_i$ is the area of the patch of S corresponding to p_i. A way to compute the values of da_i is to consider the areas of the Voronoi regions on S for each point p_i. However, for N large and the distribution of points p_i roughly uniform, the areas of these patches $d\mathbf{a}_i$ will be roughly the same. In this case, a simpler version of the discrete formula is:

$$AOF_S(\nabla D) = \frac{\sum_{i=1,\ldots,N} \nabla D(p_i) \cdot N_S(p_i)}{N}. \quad (1)$$

The above equation has been used to approximate the continuous values of the $\mathcal{AOF}$ [18] with the interpretation that large negative values indicate that a medial surface passes through S and small negative and all positive values mean that S does not contain a piece of the medial surface or that the object angle of the medial surface passing through S is small. Such interpretation is based on the assumption that the results of the continuous case as the area of S shrinks to 0 apply to the case when the area of S is non-zero.

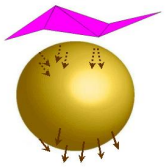

Figure 2. Inside the region S ∇D is both contracting and expanding. The AOF of ∇D over S may be greater than the negative value related to the object angle of the medial sheet that is introduced by the convex edge.

However, no matter how small S is, given an arbitrary boundary, it is always possible for ∇D to be both contracting and expanding in this small region S. For a practical example, consider Figure 2. The arrows denote ∇D vectors. In this example, a medial surface sheet passes through S because of the convex edge. However, its negative contribution to AOF is reduced by the contraction in ∇D towards the concave edge in the vicinity. This poses a serious issue for the correctness of discrete algorithms that find the medial surface based on the AOF computed using Eq. 1. Furthermore, as we will see later, even if we were assured that a medial sheet indeed passes through S, in this discrete case the relationship with the object angle may not be as stated in Table 1.

In the following discussion, we develop results that allow us to correctly apply a variant of the AOF measure in regions of non-zero size to detect medial sheets and to reason about the object angle of these surfaces for objects with a polyhedral boundary.

4. Average Outward Flux Within a Mesh

4.1. Definitions and Notation

Let B be the mesh boundary of a closed, orientable polyhedral solid. Let S be a sphere lying inside B. Here, S is the surface of the sphere.

Recall that D is the distance transform of the boundary B. $\nabla D : \mathbb{R}^3 \to \mathbb{R}^3$ is a unit vector field defined on each

point p inside the region B. Let B_p be the closest point on B to p, which is also the first intersection of a ray cast from p in the direction $-\nabla D(p)$ with B. In case of ambiguity, we pick one closest point on B arbitrarily.

Let $N_S(p)$ be the unit outward normal to S at p. Let N_f be the unit inward normal to a polygonal face f.

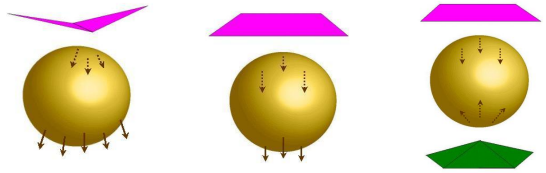

(a) (b) (c)

Figure 3. (a) 2-sided fan (b) 2-sided parallel section (c) 1-sided fan and 1-sided parallel section

In the following definitions, please refer to Figure 3 for clarification.

Definition 4.1. *A **complete fan** $F_e(S)$, or simply, **fan** of a concave edge $e \in B$ through S is defined as $F_e(S) = \{a | a \in S, B_a \in e\}$. A **fan** $F_v(S)$ of a concave vertex $v \in B$ through S is defined as $F_v(S) = \{a | a \in S, B_a = v\}$.*

We use $F_e(S)$ to refer to all fans, unless greater specificity is required.

Definition 4.2. *Let S' be a section of S. Then $S' = out(S') \cup in(S')$, where*

$$\begin{aligned} out(S') &= \{a | a \in S', \nabla D(a) \cdot N_S(a) \geq 0\} \\ in(S') &= \{a | a \in S', \nabla D(a) \cdot N_S(a) < 0\} \end{aligned}$$

Definition 4.3. *Consider a point a on S. **opp**(a) is the point of intersection of an open ray cast from a in the directions $\nabla D(a)$ and $-\nabla D(a)$ with S. In the case that $\nabla D(a)$ is tangent to S, $opp(a) = a$.*

Definition 4.4. *A **one-sided fan** $F_e^1(S)$ is a subset of $F_e(S)$ such that $F_e^1(S) = \{a | \nabla D \cdot N_S(a) < 0, opp(a) \notin F_e(S)\}$.*

Definition 4.5. *A **two-sided fan** $F_e^2(S)$ is a subset of $F_e(S)$ such that $F_e^2(S) = \{a | opp(a) \in F_e(S)\}$.*

Definition 4.6. *A **parallel section** $P_f(S)$ through S, of a face $f \in B$, is defined as $P_f(S) = \{a | a \in S, B_a \in f, \nabla D(a) = N_f\}$.*

Definition 4.7. *A **one-sided parallel section** $P_f^1(S)$ is a subset of $P_f(S)$ such that $P_f^1(S) = \{a | \nabla D(a) \cdot N_S(a) < 0, opp(a) \notin P_f(S)\}$.*

Definition 4.8. *A **two-sided parallel section** $P_f^2(S)$ is a subset of $P_f(S)$ such that $P_f^2(S) = \{a | opp(a) \in P_f(S)\}$.*

In the following we shall use AOF to refer the discrete form of the average outward flux described by Eq. 1.

4.2. Properties

Proposition 4.9. *If ∇D is parallel on S, then it is parallel inside S.*

Proof. Suppose ∇D is not parallel inside S. Then there are two points a and b inside S such that $\nabla D(a) \nparallel \nabla D(b)$. Let a_s be the point of intersection of a ray projected from a in the direction $-\nabla D(a)$ with S. Define b_s similarly. Since for both a and b $-\nabla D(a)$ and $-\nabla D(b)$ are the directions to the closest point on B, then for a_s and b_s the directions towards the closest point on B are also $-\nabla D(a)$ and $-\nabla D(b)$, which are not parallel, showing the contrapositive. □

Lemma 4.10. *Consider a pair of distinct points a and b on the surface of S such $\nabla D(a) = \nabla D(b)$ and such that a = opp(b). Then these two points contribute 0 to the AOF, i.e. $\nabla D(a) \cdot N(a) + \nabla D(b) \cdot N(b) = 0$.*

This lemma can be easily proved by considering the angles formed between $\nabla D(a)$ and $N(a)$ and between $\nabla D(b)$ and $N(b)$, and using trigonometric identities.

Proposition 4.11. *A two-sided parallel section contributes 0 to the AOF. A two-sided fan contributes positively to the AOF.*

Proof. For all points p in parallel two-sided sections P_f^2, $\nabla D(p) = N_f$. We know that $|in(P_f^2(S))| = |out(P_f^2(S))|$. Points of $in(P_f^2)$ may be uniquely paired together with points of $out(P_f^2)$ such that the contribution of each pair is exactly 0 for two-sided parallel sections, by Lemma 4.10. In the case of two-sided fan sections F_e^2, $|in(F_e^2)| < |out(F_e^2)|$. Points of $out(F_e^2)$ may not be uniquely paired up with points of $in(F_e^2)$. The total contribution of F_e^2 is positive, since the contribution $\nabla D(a) \cdot N_a$ of points a of $out(F_e^2)$ is by definition positive. □

Proposition 4.12. *One-sided parallel sections $P_f^1(S)$ and one-sided fans $F_e^1(S)$ contribute negatively to the AOF.*

Proof. By definition, $|out(P_f^1(S))| = |out(F_e^1(S))| = 0$. Therefore, the contribution to the AOF is a sum of negative $\nabla D(a) \cdot N_S(a)$ terms and the total contribution is negative. □

Proposition 4.13. *Points in S belong either to parallel sections or fans.*

Proof. For points a in S, some B_a lie on the faces of B, others lie on edges, while others lie on vertices. For those points a for which B_a lie on faces but not on edges, $\nabla D(a)$ must be normal to these faces.

We consider two kinds of edges and vertices: convex and concave. Consider a point s strictly inside B. For a convex edge or vertex of B, there is no such point p such that B_p lies on it, because there is always a point within $\epsilon > 0$ of the convex edge/vertex that is closer to p. Those points p whose closest points on B lie on concave vertices or edges are part of fans, by definition. □

Theorem 4.14. *The medial surface of the solid with boundary B passes inside the region S if and only if the AOF due to all the regions of S, except for the two-sided fans, is negative.*

Proof. [⇒] Suppose the medial surface passes through the region S inside B. Then S cannot be a two-sided parallel section, for if it were, by Proposition 4.9, ∇D would also be parallel inside S and, given that the sphere sampling rate N was large enough, no medial surface would pass through it. Note also that the situation of multiple two-sided parallel sections without a fan section is impossible. From Proposition 4.13, S contains points that belong to (two-sided and 1-sided) parallel sections and fans only. Since we know that there is a section of points in S for which ∇D is not a two-sided parallel section, there is at least one fan or one-sided parallel section. When N is large enough, we are assured to find some of these points. By Proposition 4.11, we may ignore the two-sided parallel sections, if any, since they don't contribute to the AOF. Also by Proposition 4.11, by ignoring the two-sided fans, we ignore a positive contribution to the AOF. The remaining regions – one-sided fans and parallel sections – contribute negatively, by Proposition 4.12. These regions exist because ∇D is discontinuous inside S.

[⇐] Suppose that the AOF due to all regions except for two-sided fans is negative. The remaining regions are one-sided fans and two-sided and one-sided parallel sections. By Proposition 4.11 we know that two-sided parallel sections contribute zero to the AOF. Therefore, the negative value must have come from a one-sided fan or one-sided parallel section by Proposition 4.12 and we are assured of their existence. For points a in these sections, $\nabla D(a) \neq \nabla D(opp(a))$ because otherwise both a and $opp(a)$ would share a closest point on B and would then be part of a two-sided fan or parallel section. Thus ∇D is discontinuous inside S, meaning that the medial surface passes inside S. □

Since we have established a criterion for deciding the presence of a medial surface in an area of non-zero size, it now makes sense to apply a coarse-to-fine approach in finding those areas of space where the medial surface passes. Such an approach has the distinct advantage that spatial resolution can then be increased to any desired level of detail, in the vicinity of the $\mathcal{MS}$, to efficiently obtain a highly accurate representation.

5. Coarse-to-Fine Approach

Consider a partitioning of space inside B by a regular 3D cubic lattice, each cell $C(x)$ centered at point x having size σ^3. Let $S_\sigma(x)$ be a sphere of radius σ centered at x. Let AOF' be the value of the AOF through S discounted by the contribution of the two-sided fans.

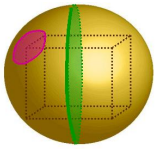

Figure 4. Intersections of a medial surface sheet with a sphere. The pink is the minimum area of intersection and the green is the maximum area.

Proposition 5.1. *If a planar section of $\mathcal{MS}$ with object angle α passes through a cell $C(x)$ that is everywhere as wide as $S_\sigma(x)$, then AOF' through $S_\sigma(x) \in [-\frac{1}{2}\sin\alpha, -\frac{1}{8}\sin\alpha]$.*

Proof. The lower bound is achieved by revisiting the case where the intersection of $S_\sigma(s)$ with $\mathcal{MS}$ is a circle of radius σ. The upper bound is obtained when $\mathcal{MS}$ passes through the corner of $C(x)$ (refer to Figure 4). In this case, the area of the circle where the medial surface cuts $S_\sigma(x)$ is $\pi(\sigma/2)^2$ and value of AOF' is $-2\frac{\pi(\sigma/2)^2}{4\pi\sigma^2}\sin\alpha = -\frac{1}{8}\sin\alpha$. □

When the medial surface is curved, the constant will increase, in part because the area of intersection to the medial surface with the sphere will be higher.

Proposition 5.2. *The thickness of those voxels which have a negative AOF' due to a sheet of the medial surface passing is at most 2.*

Proof. According to Theorem 4.14, AOF' through $S_\sigma(x)$ is negative iff there is a medial surface section passing through $S_\sigma(x)$. For those $S_\sigma(x)$ centered closer than σ of the medial surface, some portion of the medial surface passes inside. □

We may now design a coarse-to-fine algorithm for finding sections of the medial surface with a desired minimum object angle.

6. Algorithm

Given an input mesh boundary B of a 3D object, we would like to locate the significant sections of the 3D object's medial surface. We choose a desired starting resolution σ and make a 3D voxel array $Inside$ consisting of those voxels whose circumscribing spheres of radius σ fit completely inside B. We now describe our algorithm CoarseToFine.

Input: Mesh boundary B, its voxelized solid shape $Inside$ with voxel size σ^3, sphere sampling rate N, increment d, number of levels of subdivision required $levels$, object angle α.
Output: The voxels of $Inside$ subdivided $levels$ times by d through which passes a piece of the medial surface wider than $\sigma/(d^{levels})$ with object angle at least α.

Algorithm 1 CoarseToFine$(B, Inside, \sigma, N, d, levels, \alpha)$

1: **for all** voxels v of $Inside$ **do**
2: Let x be the location of v
3: Place a sphere S of radius $\sigma/(d^{levels})$ at x
4: $AOF(x) \leftarrow 0$
5: **for all** points p_i on the surface of the sphere, $i = 1 \ldots N$ **do**
6: Find the closest point y on B to p_i
7: Let $\nabla D(p_i)$ be the unit direction from y to p_i
8: Let $N_S(p_i)$ be the unit outward normal to S at p_i
9: $AOF(x) \leftarrow AOF(x) + \frac{\nabla D(p_i) \cdot N_S(p_i)}{N}$
10: **end for**
11: Let $AOF'(x)$ be the contribution to $AOF(x)$ of those points p_i that are not part of two-sided fans
12: **end for**
13: **if** $levels > 0$ **then**
14: Delete those voxels of $Inside$ located at x for which $AOF'(x) \geq 0$
15: Subdivide the remaining voxels by d^3
16: CoarseToFine$(B, Inside, \sigma, N, d, levels - 1, \alpha)$
17: **else**
18: Delete all voxels located at x of $Inside$ for which $AOF'(x) > -\frac{1}{8}\sin(\alpha)$
19: Return $Inside$
20: **end if**

Steps 3, 6 and 11 will be discussed in further detail below.

6.1. Sphere Sampling

As there are but 5 Platonic solids, the largest number of points that may be distributed uniformly on a sphere is 20, the number of vertices of a dodecahedron. When the number of points one wishes to distribute on the sphere exceeds 20, one must adopt various approximation techniques. We adopt the spherical sampling described in [17] which distributes points along uniformly-spaced vertical sections in a spiral fashion in step 3 of our algorithm.

6.2. Algorithmic Efficiency and Correctness

The most important operation of CoarseToFine is finding the closest point on B to a point on the sphere in step 6 of Algorithm 1. This must be done as efficiently as possible. Proximity queries of this sort have been studied extensively. Popular approaches use Bounding Volume Hierarchies organizing sets of geometric primitives bounded by spheres, axis-aligned or oriented bounding boxes and other bounding volumes. In our implementation, we use the Proximity Query Package (PQP) [11] for finding distances from points to the boundary. This method has been demonstrated to be quite efficient in practice, especially as it is able to capture coherence between proximity queries. Nonetheless, the calls to PQP are the most costly of CoarseToFine.

For a discussion of specific implementation details that lead to time and space savings, please refer to [19]. Also, in [19], we show that the error due to the finite sphere sampling rate is bounded.

6.3. Homotopy Type Preservation

It is known that $\mathcal{MS}$ is of the same homotopy type as Ω [14]. Coupling the extraction of $\mathcal{MS}$ with preservation of homotopy type could benefit those applications that use $\mathcal{MS}$ to study the shape of Ω. If it is desired, we delete voxels in steps 14 and 18 of Algorithm 1 only if they are *simple*, or if their removal does not change the homotopy type of the set of voxels [15]. The order in which we consider points for removal is key to obtaining a minimal set of voxels from which no other voxel with AOF' value above the given threshold may be further removed. The heuristic ordering of points for removal that we consider is that given by an approximate Euclidean distance transform where points on the boundary of the object are considered for removal before those inside.

7. Experimental Results

This section illustrates the performance of our algorithm on a number of examples.

Figure 5 demonstrates the x, y and z slices of the medial surface of a box. For this synthetic example, we observe that the value of AOF' in the middle solid section (shown darkest in the Figure) is -0.5003, which is within 0.06% of the true value of $-\frac{1}{2}\sin(\pi/2) = -0.5$. The other 8 sheets of the medial surface have AOF' value around -0.3524. For these sheets, the object angle is $\pi/4$ and the

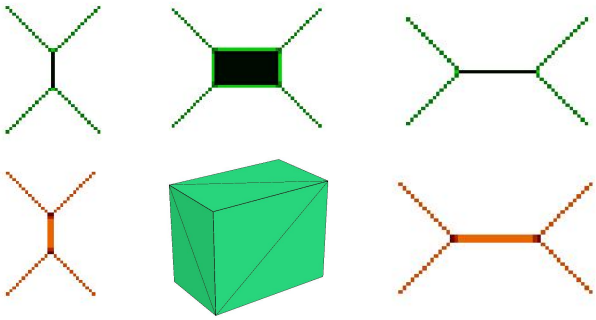

Figure 5. First row: the x, y, and z slices of the medial surface for the box with darker values representing higher AOF values. Second row: x and y slices when the medial surface passes between two voxels.

Object	Level 1	Level 2
Box	45.9%	45.5%
Venus	2.1%	12.6%
3-hole torus	3.9%	20.6%
Cow	8.5%	6.3%

Table 2. Percentage of object voxels at the highest resolution that were dismissed at each lower level of subdivision

.

AOF' value obtained is within 0.34% of the value expected of $-\frac{1}{2}\sin(\pi/4) \approx -0.3536$. The reason why the values obtain differ from the true values in this synthetic case is because of the finite sphere sampling. Here, the medial surface passes right through the centre of the voxels and the medial surface is one voxel thick. When the medial surface passes between two voxels, as in the last row of Figure 5, the value of AOF' in the middle section is -0.3315. This is due to the particular choice of discretization of space and is an inherent feature of methods relying on discretization.

Table 2 summarizes the computational savings when using 3 levels of recursive subdivision. The subdivision factor d used was 3 and the sphere sampling rates were 70, 60, and 50, for the low, middle, and high resolutions respectively.

We compare our output with that of a known medial surface algorithm, the PowerCrust [2] in Figures 6 and 7. The input to the PowerCrust is the set of mesh vertices. Qualitatively, the examples show that our algorithm can yield smooth manifolds due to the fact that the voxel grid can be subdivided to the desired level of resolution.

8. Conclusions and Future Work

We have presented an approach to detect regions of space containing the medial surface of a polyhedral object. By relying as much as possible on exact computations and applying the necessary criterion for correctness, our method is able to compute the location of the medial surface with arbitrary precision.

It turns out that a complete characterization of the differential geometry of an object's surface is possible in terms of a radial shape operator on the medial surface [7]. Furthermore, medial and skeletal integrals can be used to compute fundamental geometric quantities as described in Damon's pioneering recent work [6]. Our current work is focused on adopting these continuous measures for use with our medial surface algorithm for polyhedra.

Acknowledgments

We would like to thank Sue Whitesides and the reviewers for their helpful comments. We would also like to thank Dinesh Manocha for providing us with the PQP source code and Nina Amenta for making the PowerCrust code publicly available. This work is supported by grants from NSERC and FQRNT.

References

[1] D. Attali, A. Montanvert. Computing and Simplifying 2D and 3D Semicontinuous Skeletons of 2D and 3D shapes. *CVIU*, 67(3): 261-273, 1997.

[2] N. Amenta, S. Choi, R. K. Kolluri. The power crust. *ACM Symposium on Solid Modeling and Applications*, 249-260, 2001.

[3] I. Boada, N. Coll, N. Madern, J. A. Sellarès. Approximations of 3D generalized Voronoi diagrams. *EWCG2005*, 2005.

[4] H. Blum. Biological shape and visual science. *Journal of Theoretical Biology*, 38: 205-287, 1973.

[5] T. Culver, J. Keyser, D. Manocha. Exact computation of the medial axis of a polyhedron. *Computer Aided Geometric Design*, 21(1): 65-98, 2004.

[6] J. Damon. Global geometry of regions and boundaries via skeletal and medial integrals. Preprint.

[7] J. Damon. Determining the geometry of boundaries of objects from medial data. *IJCV*, 63(1):45-64, 2005.

[8] P. Dimitrov, J. N. Damon, K. Siddiqi. Flux invariants for shape. *CVPR*, 2003.

[9] M. Etzion, A. Rappoport. Computing Voronoi skeletons of a 3-D polyhedron by space subdivision. *Computational Geometry: Theory and Applications*, 21:87-120, 2002.

[10] M. Foskey, M. C. Lin, D. Manocha. Efficient computation of a simplified medial axis. *Symposium on Solid Modeling and Applications*, 96-107, 2003.

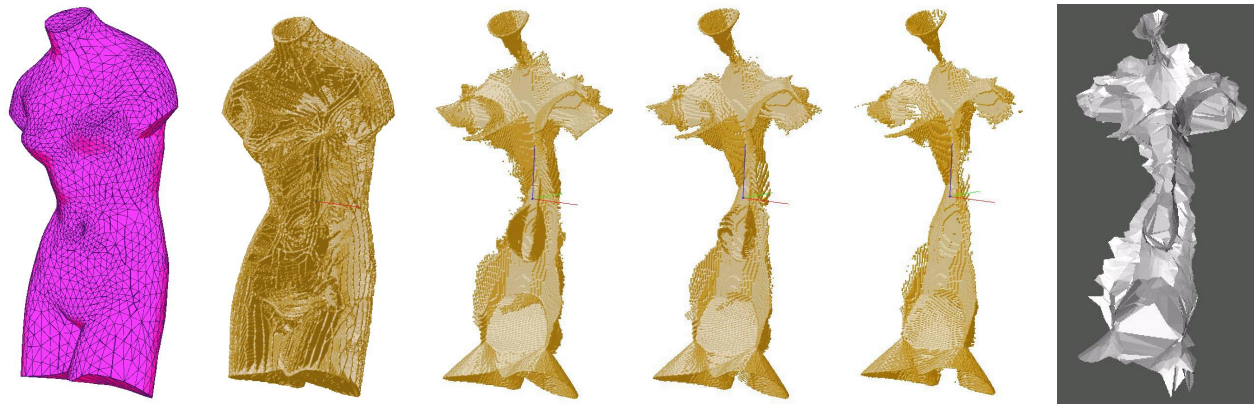

Figure 6. Left to right: the "Venus" mesh (5672 triangles) and its medial surface at a resolution of $177 \times 129 \times 361$ voxels: the full medial surface, voxels with AOF' values below -0.15, -0.2, and -0.25, and the medial surface produced by the PowerCrust [2].

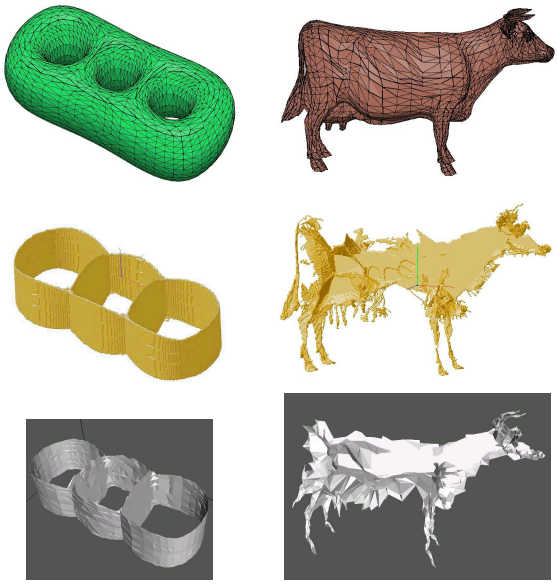

Figure 7. Left (top to bottom): a three-hole torus (4000 triangles) and those internal voxels whose AOF' is below -0.22 with resolution $369 \times 173 \times 128$ voxels. Right (top to bottom): a cow mesh (5804 triangles) and its $\mathcal{MS}$ with homotopy type preserved with resolution $369 \times 227 \times 121$ voxels. Voxels with AOF' below -0.2 were eligible for removal. The last row is produced by the PowerCrust [2].

[11] E. Larsen, S. Gottschalk, M. C. Lin, D. Manocha. Fast proximity queries with swept sphere volumes, Technical report TR99-018, Department of Computer Science, University of N. Carolina, Chapel Hill, 1999.

[12] F. Leymarie, B. Kimia. Computation of the shock scaffold for unorganized point clouds in 3D. *CVPR*, 821-827, 2003.

[13] F. Leymarie, B. Kimia. The shock scaffold for representing 3D shape. *IWVF4*, 2001.

[14] A. Lieutier. Any open bounded subset of $\mathbb{R}^n$ has the same homotopy type than its medial axis. *ACM Symposium on Solid Modeling and Applications*, 65-75, 2003.

[15] G. Malandain, G. Bertrand. Topological segmentation of discrete surfaces. *CVPR*, 444-449, 1991.

[16] S. M. Pizer, K. Siddiqi, G. Szekely, J. N. Damon, S. W. Zucker. Multiscale medial loci and their properties. *IJCV*, 55(2-3): 155-179, 2003.

[17] E. B. Saff, A. B. J. Kuijlaars. Distributing many points on a sphere. *Mathematical Intelligencer*, 19(1):5-11, 1991.

[18] K. Siddiqi, S. Bouix, A. R. Tannenbaum, S. W. Zucker. Hamilton-Jacobi skeletons. *IJCV*, 48(3):215-231, 2002.

[19] S. Stolpner. Exact coarse-to-fine medial surfaces. Master's thesis, School of Computer Science, McGill University, in preparation.

[20] A. Sud, M. Foskey, D. Manocha. Homotopy-preserving medial axis simplification. *Symposium on Solid and Physical Modeling*, 39-50, 2005.

[21] R. Tam, W. Heidrich. Shape simplification based on the medial axis transform. *IEEE Visualization*, 481-488, 2003.

[22] J. Vleugels and M. Overmars. Approximating generalized Voronoi diagrams in any dimension. Technical report UU-CS-1995-14, Department of Computer Science, Utrecht University, 1995.

[23] J. Zhang, K. Siddiqi, D. Macrini, A. Shokoufandeh, S. Dickinson. Retrieving articulated 3-D models using medial surfaces and their graph spectra. *International Workshop On Energy Minimization Methods in Computer Vision and Pattern Recognition*, 2005.